Optical Materials: X 7 (2020) 100055

Contents lists available at ScienceDirect

Optical Materials: X

journal homepage: www.journals.elsevier.com/optical-materials-x

SERS in red spectrum region through array of Ag–Cu composite nanoparticles formed by vacuum-thermal evaporation

S.V. Dubkov [a,*], A.I. Savitskiy [c], A. Yu Trifonov [a,e], G.S. Yeritsyan [c], Yu.P. Shaman [c], E. P. Kitsyuk [c], A. Tarasov [a], O. Shtyka [d], R. Ciesielski [d], D.G. Gromov [a,b]

[a] National Research University of Electronic Technology, Zelenograd, Russia
[b] I.M. Sechenov First Moscow State Medical University, Moscow, Russia
[c] Scientific-Manufacturing Complex "Technological Centre", Zelenograd, Russia
[d] Institute of General and Ecological Chemistry, Lodz University of Technology, Lodz, Poland
[e] Scientific Research Institute of Physical Problems Named After F.V.Lukin, Zelenograd, Russia

ARTICLE INFO

Keywords:
SERS
Nanoparticles
Ag–Cu
Silver
Copper
Alloy

ABSTRACT

In order to expand the spectral capabilities of the SERS method, Ag–Cu alloy nanoparticle arrays were studied. Arrays of Ag–Cu nanoparticles were formed by vacuum thermal evaporation and condensation on an unheated substrate followed by heat treatment at 230 °C. A higher Raman scattering enhancement in the red region of the spectrum when using an array of nanoparticles of the Ag–Cu eutectic system was found. This enhancement is comparable to the one of pure silver particle array in the blue region of the spectrum. Transmission electron microscopy study has shown that the feature of the Ag–Cu array is that many particles are composite: one part consists of copper, and the other part is made up of silver. These parts have a perfect (possibly heteroepitaxial) boundary. It is believed that the localized surface plasmon resonance excited in the copper part by red light can be transmitted without any loss into the silver part, while the one excited in the silver part by blue light, quickly fades out in the copper part, because blue light has a higher frequency than the copper plasma frequency. From the point of view of SERS applications, the use of Ag–Cu particle arrays allows extending the advantage of silver to the red region of the spectrum.

1. Introduction

Plasmonics of metal nanoparticles, which is based on the phenomenon of localized surface plasmon resonance (LSPR), is a rapidly growing and expanding field of research due to wide prospects for its use [1–7]. LSPR occurs when the frequency of the incident radiation is equal to the natural frequency of collective oscillations of conduction electrons in an array of metallic nanoparticles. As a result, the absorption of photons of this energy is observed. In this case, the occurrence of resonant oscillations of free electrons actually generates hot charge carriers (electron-hole pairs) with energy of 1–3 eV [8]. These hot charge carriers have a short lifetime of about several femtoseconds and are not in thermal equilibrium. If the incident radiation is removed, carrier recombination ends in a few picoseconds, and complete relaxation occurs in tens of nanoseconds [8]. That means that in normal situation this process is very rapid, and it is difficult to apply it anywhere. However, if semiconductor molecules are placed on the top of the metal nanoparticles array, this, in fact, can lead to the formation of a Schottky barrier capable of separating hot electrons and holes generated by the incident radiation. In this case, the carrier lifetime increases significantly. And then these charge carriers are involved in the occurrence of a number of phenomena, such as giant Raman scattering (Surface Enhanced Raman Scattering – SERS) [9], luminescence enhancement [10–12], or photocatalysis of various chemical processes [13–15].

The Raman spectrum arises as a result of interaction of an incident high-frequency wave with the relatively low-frequency oscillations of the dipole moment of the atoms in the molecule or in the crystal lattice and, in fact, is a "modulation" phenomenon [16]. A hot carrier of the metal nanoparticle may be captured by the molecule. This leads to the emergence of a molecular ion from the surface molecule [9] and, thereby, to an increase in the dipole moment. As a consequence, the amplitude of the modulating signal, which is the Raman signal, is amplified, i.e. SERS occurs. However, this option is only available for semiconductor materials, which are characterized by a donor-acceptor

* Corresponding author.
E-mail address: sv.dubkov@gmail.com (S.V. Dubkov).

https://doi.org/10.1016/j.omx.2020.100055
Received 15 April 2020; Received in revised form 26 May 2020; Accepted 31 May 2020
Available online 22 June 2020

bond type and a bandgap no greater than the energy of the generated hot charge carriers. In the materials with ionic bonds which are characterized by a very large band gap and a complete absence of free charge carriers this process is hardly possible. Such materials are originally characterized by the presence of a strong dipole moment. Obviously, in this case, oscillations of the dipole moments of the molecules are transferred to the free electrons of the metal particle, creating a low-frequency wave in it. The interaction of the plasmon generated in the metal particle by an incident high-frequency light wave, with the low-frequency wave transmitted to the metal particle from the molecule under study then leads to the modulation of a light wave. The enhancement arises due to an increase in the efficiency of interaction of two waves by increasing the interaction area, that is, due to an increase in modulation efficiency.

Traditional materials for plasmonic arrays of metal particles are Ag, Au and Cu. But Ag particles have the strongest enhancement. This result is achieved when the light in the range from blue to UV is used. However, in the substance under investigation luminescence can often occur. As noted above, an array of metal nanoparticles enhances this effect as well. Then the desired Raman signal can be lost against the background of luminescence. To get rid of this effect, it is necessary to choose a different reference light wavelength and another array of metal nanoparticles with the corresponding position of LSPR. It is possible to choose Au or Cu particles. It is also possible to use Ag–Au alloy particles, since their composition allows controlling the position of the LSPR smoothly [17,18]. The problem is that when using Au, Cu and Ag–Au particles the amplification is noticeably weaker. Thus, it is desirable to have a method of changing the reference wavelength without losing the enhancement of the Raman signal. In this regard, arrays of composite particles may be of interest. It was shown that significant amplification of the Raman signal is provided by using alloy dendrites [19–23], alloy and bimetallic core-shell nanoparticles [21,22,24–26]. Such structures can be synthesized using various approaches: electrodeposition, phased reduction, laser ablation, and self-assembly methods [21,22,25–29]. Among the composite materials, the Ag–Cu system is of particular interest.It is expected that SERS structures based on this composite will be more stable [25,27], cheaper due to the use of copper and more universal in terms of the wavelength range and gain [21,22,25,26,30].

Ag–Cu system has an eutectic phase equilibrium diagram [31]. A feature of eutectic systems is that eutectic composition in the solid state consists of two highly dispersed solid solutions based on the system components, and these solutions contact with each other. So far, no detailed studies of the relationship between the structure of Ag–Cu particles and the effect of amplification of the Raman signal depending on the wavelength have been carried out.

This paper is devoted to the study of the possibility of using of an array of particles based on the Ag–Cu system, whose components have eutectic phase equilibrium diagram, as the SERS-active layer at three different laser wavelengths. In other studies, arrays of Ag–Cu nanoparticles were obtained by method of chemical formation from solutions [32] or by laser ablation method [25,33]. However, the process of transferring these particles to the surface of the substrate to form an array is poorly reproducible. Often particles randomly accumulate in an uncontrolled manner in agglomerates [25,34,35]. In this regard, we have chosen the method of thermal evaporation in vacuum for our research [36–38]. Although the particles in such arrays have different sizes, nevertheless, their size distribution is normal; statistics on the average particle size and the distance between them are well controlled and reproduced. In this regard, we have chosen the method of thermal evaporation in vacuum for our research [36–38]. Although the particles in such arrays have different sizes, nevertheless, their size distribution is normal; statistics on the average particle size and the distance between them are well controlled and reproduced.

2. Experiment

The formation of Ag–Cu nanoparticles arrays was carried out by vacuum thermal evaporation of the weight portions of the corresponding metal onto a cold substrate with subsequent annealing of the obtained condensate in vacuum. In previous works we reported in detail on the applicability of this technique for the formation of metal particles arrays on the planar structures, as well as on the possibility of controlling the average particle size and their number per surface unit [36–38]. In this study, there has been evaporated a weight portion of 2.8 mg to obtain silver nanoparticles, and a weight portion of 6.0 mg to obtain an ensemble of copper particles. Vacuum annealing of the copper condensate was carried out during 1 h at temperature of 500 °C. For silver the annealing temperature was 230 °C, and the duration was 30 min. The difference in the annealing parameters is due to the fact that upon evaporation of such a quantity of silver, the resulting condensate is an unstable islet film, which is transformed into an array of nanoparticles after slight heat treatment. At the same time, the evaporation of the specified copper weight portion leads to the formation of a continuous film, and its dispersion requires a greater thermal effect [39]. It is worth noting that, despite some differences in the formation approaches, both methods provide good reproducibility of geometric parameters of the resulting arrays of particles. For the formation of Ag–Cu nanoparticles ensembles, the technique of co-evaporation of weight portions of metals has been used, which was successfully tested earlier on other two-component systems [28,40]. The choice of the weight portions ratio of Ag (4.0 mg) and Cu (1.6 mg) is due to the desire to obtain a condensate of eutectic composition (~39.9 at.% of Cu). Annealing of the obtained condensate was carried out at the temperature of 300 °C for 30 min. For all vacuum processes at the nanoparticle formation stage, the residual pressure in the chamber was not worse than $1{\cdot}10^{-5}$ Torr.

The arrays of nanoparticles were studied using FEI Tecnai G^2 20 S-Twin transmission electron microscope (TEM) equipped with EDAX company system for X-ray energy dispersive spectroscopy (EDX). The analysis of the obtained images allowed us to construct a histogram of the distribution of particles depending on their size. Using histograms, the average size of the array particles and the number of particles per unit area (surface density) were determined. PHI 5000 VersaProbe II photoelectron spectrometer with a monochromatized source of excitation by Al K_α radiation ($h\nu = 1486.6$ eV, power 50 W, diameter 200 μm) was used to determine the surface chemical composition and valence states of Ag–Cu nanoparticles.

The samples with particle arrays for spectrophotometric studies were formed on 1200 μm thick glass substrates with the surface roughness of ~3 nm. The substrates underwent standard chemical treatment in the solution of Karo and ammonium peroxide to remove organic and inorganic contaminants, followed by washing in deionized water and drying under nitrogen. In the studied range, the transmittance of the glass used in the experiment was approximately 90%. The transmission spectra of such samples were measured using SF-2000 spectrometer in the wavelength range of 0.35–1.00 μm. To present the results, the transmission spectrum of the glass was subtracted from the measured spectrum. To evaluate the effectiveness of the use of the formed nanoparticles arrays in SERS diagnostics, there was manufactured a series of planar SERS substrates similar to the substrates used in Ref. [17]. Their structure contained several functional layers: a single crystal Si substrate, a reflecting 100 nm thick Al layer, an intermediate 20 nm thick SiO_2 layer, and a SERS active layer of an array of nanoparticles discussed above.

Before the formation of the functional layers, the substrates underwent standard chemical treatment. Thereafter, reflecting Al layer and SiO_2 layer were sequentially formed in one vacuum cycle in the magnetron and electron beam deposition facility EvoVac (Angstrom Engineering Company). The layer deposition rate was ~1 Å/s. The value of the residual pressure in the chamber did not exceed $1{\cdot}10^{-6}$ Torr. Then, an array of nanoparticles was formed on the surface of the deposited SiO_2 layer.

At the final stage of the sample formation by magnetron sputtering, the array of nanoparticles was covered with 25 nm thick amorphous carbon film. A 25 nm thick amorphous carbon film was chosen as the analyte for several reasons. It is equally transparent (~95%) in the entire studied wavelength range. The a-C film, formed by magnetron sputtering, is highly continuous and uniform in thickness (thickness variation is ~5%). In addition, they are very well studied [41]. Since the difference between SERS structures in this paper lies only in the SERS active layer used, the intensity of amorphous carbon spectral lines allows us to judge the efficiency of using each of the particle arrays.

To obtain Raman spectra from the layers of amorphous carbon, the Raman spectrometer LabRAM HR Evolution with 600 mm^{-1} diffraction grating was used. In order to reveal the correspondence between the efficiency of Raman scattering and optical characteristics of the formed arrays, measurements were taken at three different exciting radiation wavelengths: 488, 514 and 633 nm. For this purpose, a tunable wavelength Melles Griot IMA101040 ALS argon laser and Melles Griot 05-LHP-928 helium-neon laser were used. The measurement parameters were similar to Ref. [17].

3. Results and discussion

Fig. 1 shows TEM images of arrays of pure Ag nanoparticles and bi-component Ag–Cu nanoparticles, as well as the corresponding histograms of array particles size distribution. As can be seen in the distribution diagrams for an array of silver and Ag–Cu particles, the average particle size is close to 30 nm. Nanoparticles in the array of pure Ag are closer to spherical, while nanoparticles in the Ag–Cu array have an elongated and irregular shape. Actually, this is the reason why the particle size distribution diagram of this array is non-uniform: the error of determining the particle size is quite large. Statistical image processing of these arrays gives the following results: the average particle size of pure silver is 30.1 nm and the standard deviation is 7.7 nm, while the average particle size of Ag–Cu is 34.2 nm and the standard deviation is 19.3 nm. Thus, the lower homogeneity of Ag–Cu particles compared to pure Ag particles is manifested in a larger standard deviation (56.4% versus 38.2%).

We do not give here the image of the array of pure copper nanoparticles, because it was not possible to obtain such TEM sample by our method: copper particles almost completely oxidized by immersing the sample in water to dissolve the salt substrate.

The chemical compositions of Ag–Cu particles surface were analyzed by X-ray photoelectron spectroscopy (XPS). The carbon lines of the substrate coating, gold and silver lines of alloy particles distributed in the coating and the oxygen line are present in the spectrum recorded in the area of 200 μm in diameter. The atomic concentrations of gold and silver were equal. The chemical state of silver was determined using the spectra of Ag3d and AgMNNas shown in Fig. 2. The binding energy of Ag3d 5/2 peak was 368.2 eV. M5N45N45 is an Auger peak corresponding to the transition of an electron from the level N45 (Ag4d) to the level M5 (Ag3d5/2) with the release of energy EM5 - EN45 and subsequent electron emission from the level N45.M4N45N45 is an Auger peak corresponding to the transition of an electron from the level N45 (Ag4d) to the level M4 (Ag3d3/2) with the release of energy EM4 - EN45

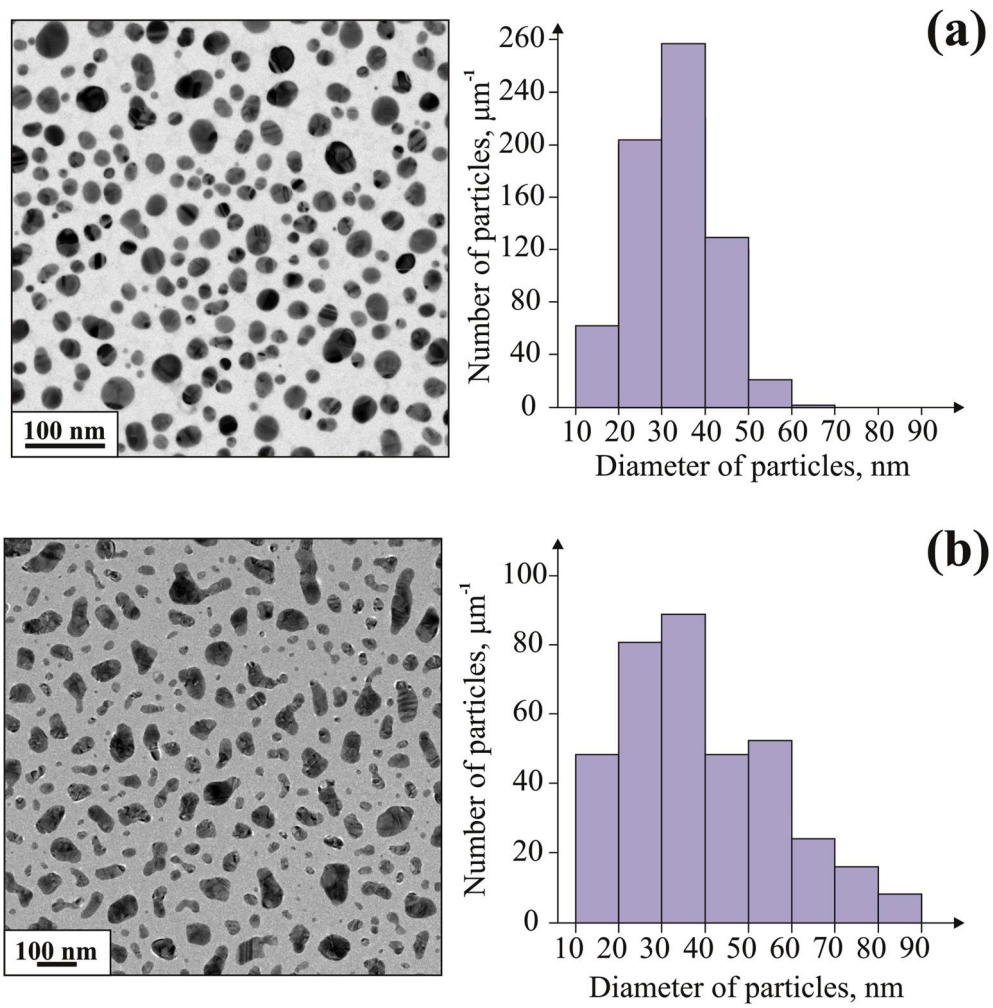

Fig. 1. TEM images and particles size distribution histograms of silver (a) and Ag–Cu (b) nanoparticles arrays.

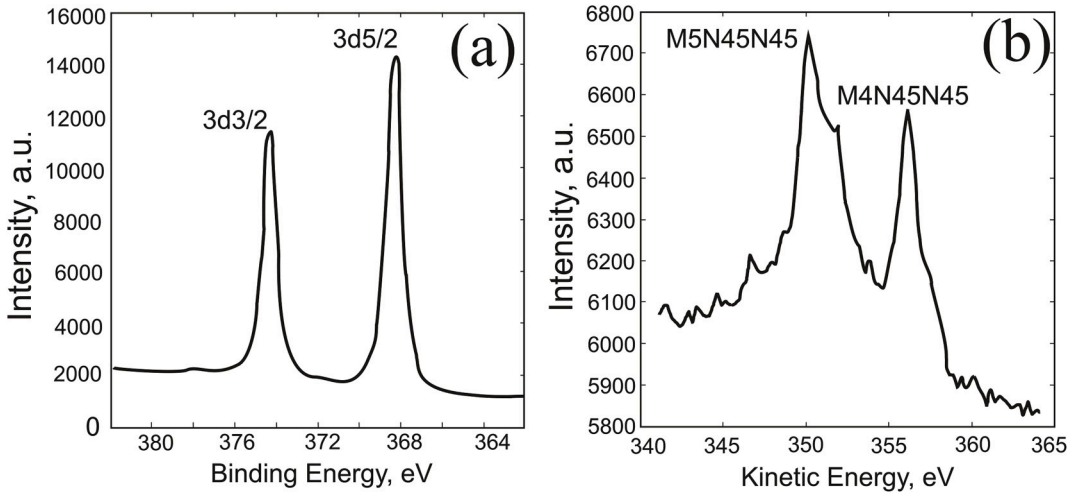

Fig. 2. High-resolution Ag3d (a) and AgMNN (b) XPS spectra of Ag–Cu particle.

and subsequent electron emission from the level N45.To calculate kinetic energy, the peak M4N45N45 was used, because it is sharper and gives higher accuracy. The Auger parameter α′, determined from the peak of M4N45N45, amounted to 726.0 eV, which corresponds to the metallic silver Ag^0. The Cu2p spectrum is shown in Fig. 3(a). The presence of plasma loss satellites indicates the presence of a CuO layer. The approximation of the Cu2p3 peak revealed two peaks: peak 1 (932.6 eV) and peak 2 (933.8 eV), which corresponds to divalent copper Cu^{2+} in CuO, as can be seen from Fig. 3(b). Its share is approximately 30–40%. Peak 1 can correspond to both Cu^0 of metallic copper and $Cu^{1+}$of Cu_2O; separating these states by the Auger parameter α′ is impossible due to superposition of the CuLMM and Ag3p3 lines. Thus, using XPS, it was found that the resulting array of Ag–Cu nanoparticles consists only of metallic silver and partially oxidized metallic copper.

Studies of Ag–Cu and pure Ag particle arrays in electron diffraction mode (Fig. 4) showed that in the case of Ag particle array (Fig. 4(a)), only diffraction rings from the fcc lattice with the parameter strictly corresponding to the lattice parameter of silver can be observed on the electron diffraction pattern. In the case of Ag–Cu array, a combination of the rings of two Ag and Cu lattices is present on the electron diffraction pattern, although the Cu rings are less intense. This is quite natural, since the conceived eutectic composition corresponds to 40 at.% Cu and 60 at.% Ag [31]. In addition, the molar mass of Ag is 1.7 times greater than the mass of Cu. Fig. 5 presents the results of studying the sample in the scanning transmission electron microscopy mode (STEM) using a high-angle annular dark field detector (HAADF) in combination with EDX method. On the elemental maps it is clearly seen that most nanoparticles are composite, i.e. consist of copper and silver parts. Due to Z-contrast, these parts also differ in brightness in the HAADF-STEM image.

To visualize the distribution of copper in a single particle, a dark-field image mode has been used. The most intense diffraction spots of copper 111, corresponding to the interplanar distance $d = 0.208$ nm, are very close to 200 silver spots ($d = 0.204$ nm). In particular, in the diffraction pattern of Fig. 2 (b), the corresponding rings practically merge. Therefore, to build a dark field image shown in Fig. 6 (a) the copper reflex 200 was used, corresponding to the interplanar distance $d = 0.180$ nm. As a result, the copper part (Fig. 6 (a)) of the particle shown in Fig. 6 (b) as bright-field image can be clearly seen. The quality of the Ag/Cu boundary can be estimated in the high resolution image (Fig. 7). It is possible to distinguish a region with a silver lattice (1) and a twin with a copper lattice (2 and 3). The boundary between them is clear enough. This suggests that in this case there is a heteroepitaxial boundary between silver and copper.

When analyzing the phase equilibrium diagram of this system [31], the fact that the nanoparticles are composite and consist of both copper and silver at the same time seems quite natural. A feature of eutectic alloys is that their constituent elements do not mix (there is only limited

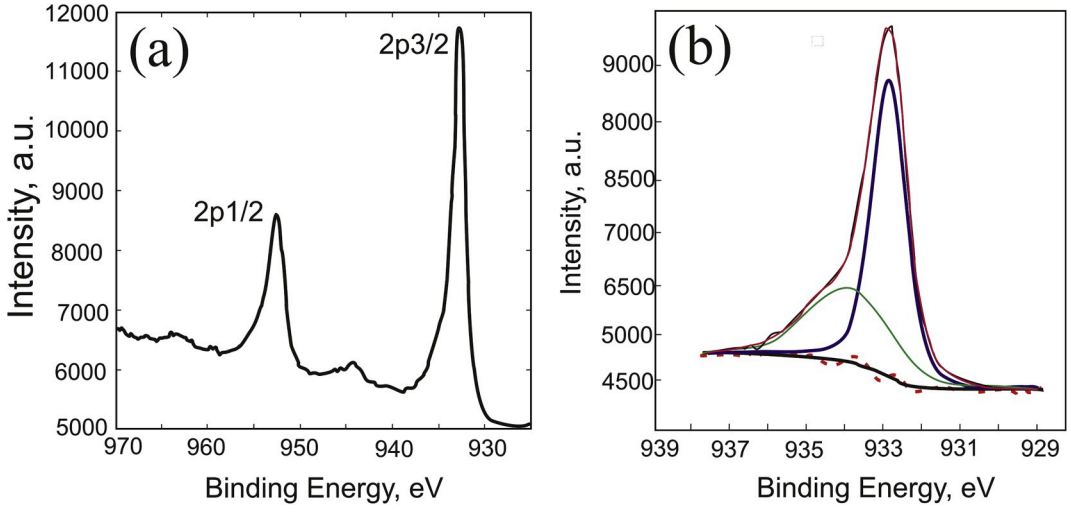

Fig. 3. High-resolution Cu2p (a) and Cu2p3 (b) XPS spectra of Ag–Cu particle.

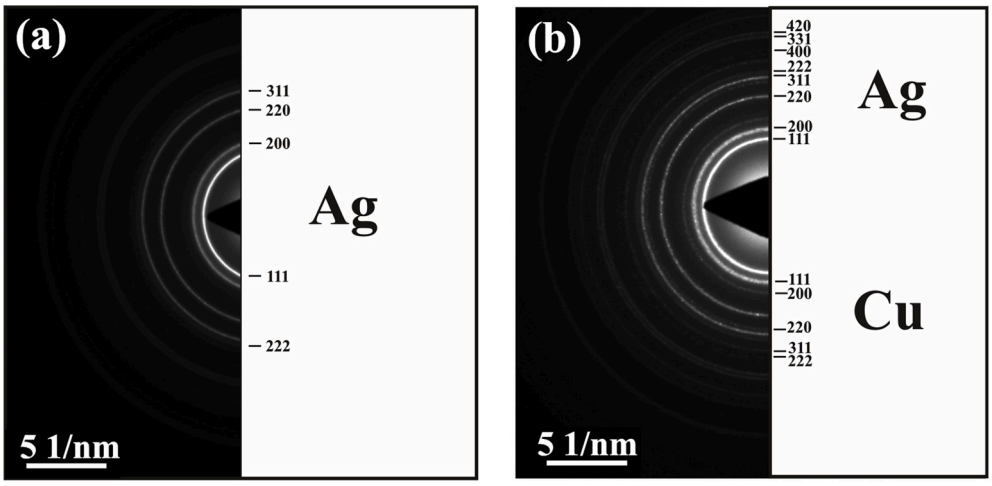

Fig. 4. Selected area diffraction patterns of silver (a) and Ag–Cu (b) nanoparticles arrays.

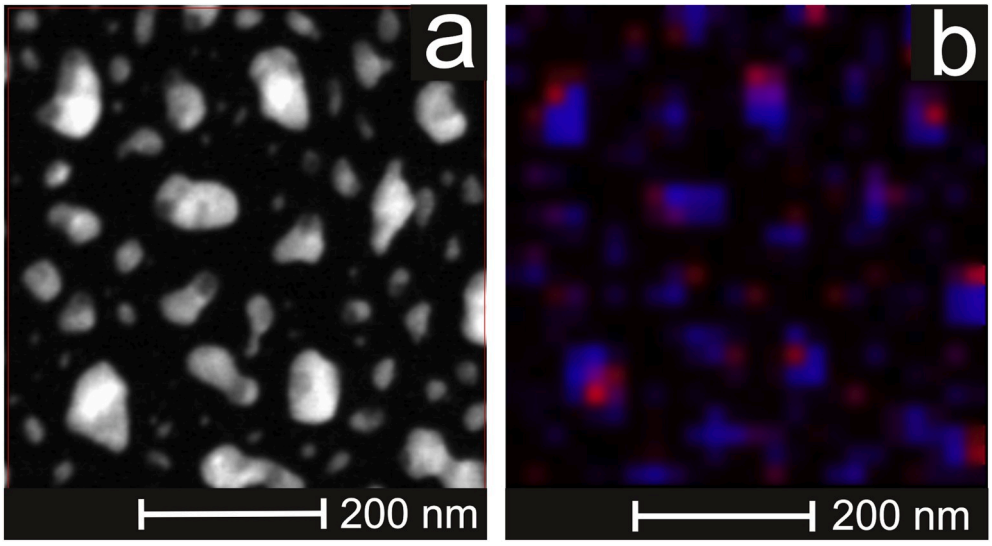

Fig. 5. Fragmented STEM image of the studied array of nanoparticles (a); EDX elemental maps of this fragment (b), where copper is shown in red and silver in blue. (For interpretation of the references to colour in this figure legend, the reader is referred to the Web version of this article.)

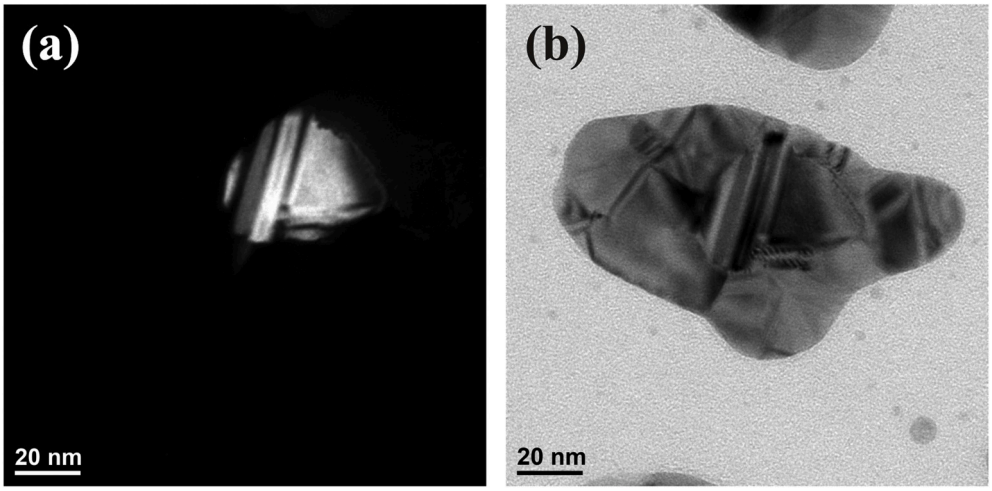

Fig. 6. (a) Dark field TEM image of Ag–Cu particle. To build this image the diffracted beam corresponding to (200) planes of copper lattice was used. (b) Bright field image of the same particle.

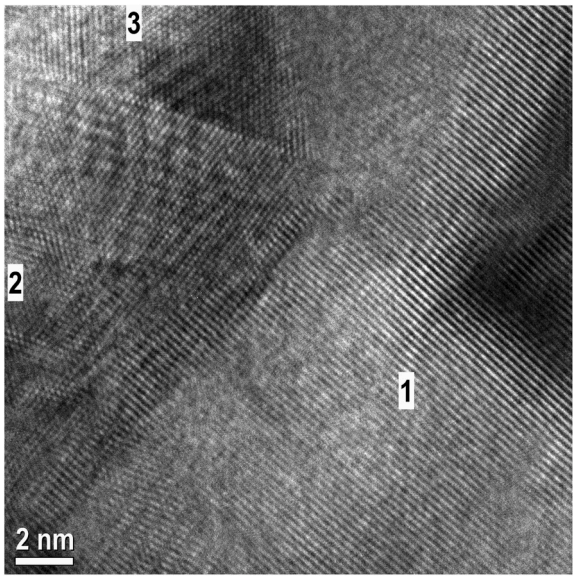

Fig. 7. High resolution TEM image of Ag–Cu particle. (1): planes (111) of Ag crystal lattice. (2) and (3): twin crystal of copper.

solubility in each other). At the same time, it is necessary to emphasize that they are very prone to contact with each other. As a result, the two-phase region in the solid state for these alloys consists of two solid solutions based on one and the other component with a very advanced interfacial contact area. Therefore, in the nanoscale region these two materials Ag and Cu still prefer to remain in contact with each other even at the level of nanoparticles. A composite particle is a eutectic at the nanoscale. The authors [25] did not have enough detail to see this clearly. But Malviya and Chattopadhyay [33] when using laser ablation observed a situation similar to our result.

Fig. 8 shows the transmission spectra of metal particles arrays with an average size of ~25–30 nm. As can be seen, the transmission minimum due to LSPR is at the wavelength of ~415 nm for Ag array, and at ~580 nm for Cu. For a combined array of Ag–Cu particles, the transmission spectrum has two minima: slightly shifted to the long-wavelength region by 460 nm corresponding to silver and slightly shifted to the short-wavelength region by 570 nm corresponding to copper. Thus, the position of the LSPR in this case somewhat did not coincide with the laser wavelength of our spectrophotometer.

The Raman spectra of the amorphous carbon thin film (20 nm) on the

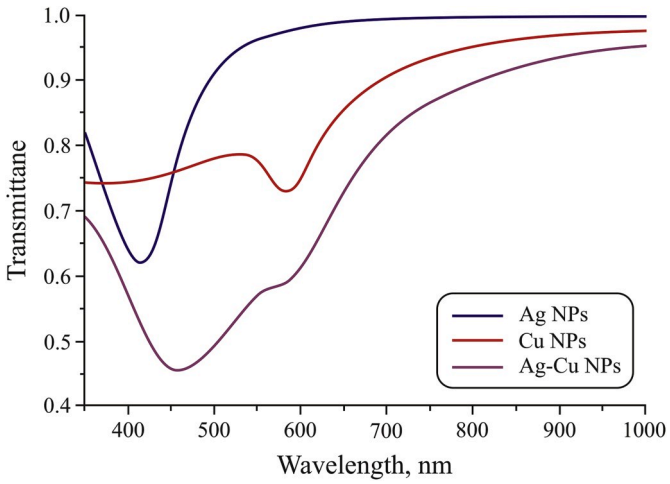

Fig. 8. The transmission spectra of the obtained arrays of Ag, Cu, and Ag–Cu nanoparticles on glass substrates.

studied nanoparticle arrays are shown in Fig. 9. As expected, the maximum amplification of the Raman signal for an array of Ag particles is observed for blue laser, whose wavelength of 488 nm is closest to the position of the LSPR for this array. When moving away from this position into the long-wavelength region, the enhancement efficiency naturally decreases. On the arrays of Cu nanoparticles, the amplification of the Raman signal as a whole turned out to be much lower, which can be associated with the rapid oxidation of copper nanoclusters. There are reports that oxidation of Cu to CuO or Cu_2O leads to degradation of plasmonic properties [42,43]. As it can be seen, the advantage of the Ag–Cu alloy compared to Ag is that it amplifies the Raman signal well in a wide range of wavelengths, including the red region of the spectrum, which is most important. For the wavelength of 514 nm the enhancement efficiency of the Ag–Cu array in our experiment turned out to be even higher than that of the Ag array. However, the enhancement factor (EF) that was calculated using a well-known technique [44] was $1{\cdot}10^4$ for Ag at 488 nm and $7{\cdot}10^3$ for Ag–Cu alloy at 633 nm. The enhancement on Ag particles was slightly higher than on Ag–Cu alloy particles. Such values of EF are typical to SERS probe of amorphous carbon as a study object [17]. The estimation of the measurement error for the a-C film (1580 cm^{-1}) on Ag, Cu, and Ag–Cu nanoparticles (Fig. 9(d)) showed that the values of the relative standard deviation (RSD) do not exceed 9.2%, 4.2%, and 10.7% respectively.

Nevertheless, the Raman spectra obtained on the arrays of combined Ag–Cu nanoparticles demonstrate the most interesting results. Two facts are noteworthy here:

- the maximum Raman scattering enhancement on the arrays of combined Ag–Cu nanoparticles turned out to be for red laser, whose wavelength of 633 nm is closest to the position of the LSPR of the copper nanoparticle array;
- The Raman scattering enhancement efficiency of the Ag–Cu nanoparticles at 633 nm was comparable with the amplification of pure silver nanoparticles at 488 nm.

Despite the unexpectedness of the result, the explanation seems to be quite simple and hidden in the composite nature of Ag–Cu nanoparticles, which was shown above in TEM study results (Figs. 5–7). Probable heteroepitaxial boundary Ag/Cu within the particle provides a good electrical contact between Ag and Cu parts. In fact, this means that such a particle has a unified collective community of free electrons. The difference consists only in different nature of interaction of this free electrons community with the potential fields of the crystal lattices of copper and silver. In particular, the plasma frequency of copper is in the red region of the spectrum, while the plasma frequency of silver is in the blue region. As it is well known from metal optics, below this frequency electrons oscillate strictly reproducing the frequency of the incident radiation; however, above this plasma frequency the metal electrons no longer have time to oscillate in accordance with the frequency of the incident radiation. In our case of a composite particle, this means that when exposed to red light, due to a single collective community of free electrons, the resonant plasmon excited in the copper part of the particle will spread in the silver part of the particle without any difficulty (or with even lower attenuation, since the electron mean free path in silver is greater than in copper). At the same time, when exposed to blue light, the resonant plasmon, excited in the silver part of the particle, will damp out in the copper part. As already noted above, the frequency of the silver resonant plasmon is higher than the plasma frequency of copper, and the free electrons in the copper part of the particle will not have time to oscillate according to the frequency of the silver plasmon.

In the introduction we referred to papers [19,20]. They studied SERS on Ag–Pt and Au–Pd alloys. It was shown that EF in alloys is greater than that in pure Ag and Au, respectively. From the point of view of the above and the nature of the material itself, any alloy should concede to pure metal, especially silver, since any addition of impurity atoms to the crystal lattice violates its periodicity and leads to an increase in the

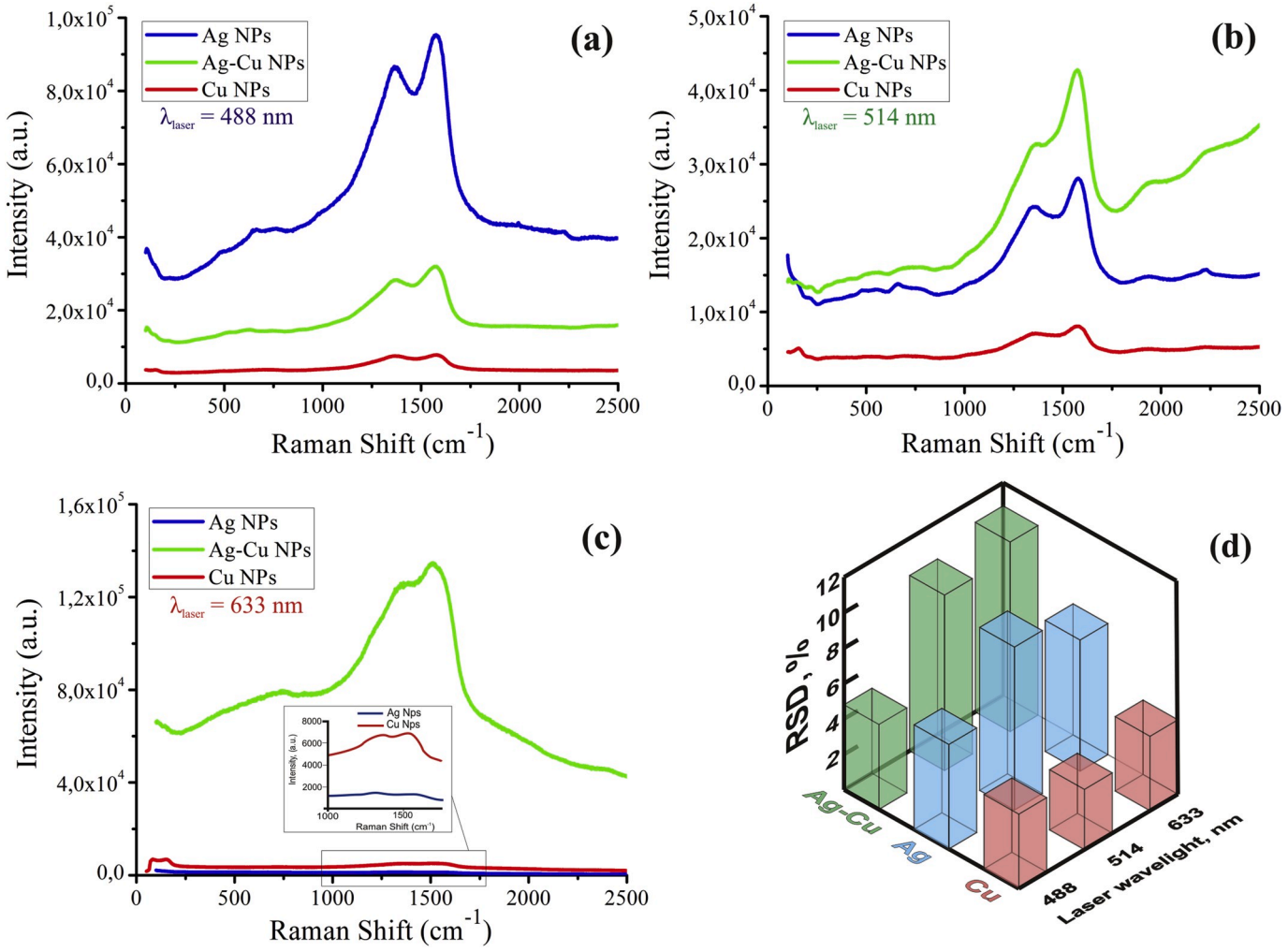

Fig. 9. Raman spectra of amorphous carbon thin films deposited on SERS structures based on arrays of Ag, Cu and Ag–Cu nanoparticles using lasers with the wavelengths of 488 (a), 514 (b) and 633 nm (c); reproducibility of the SERS intensities for a-C film (1580 cm^{-1}) on Ag, Cu и Ag–Cu NPs SERS substrate. The histogram shows the estimated RSD values (d).

scattering efficiency of free electrons and, consequently, to the loss of their energy. This affects plasmon resonance, and should cause a decrease in Raman scattering enhancement. Nevertheless, the increase in EF observed for alloys in Ref. [19,20] can be associated with another factor important for SERS – the form factor. So in Ref. [19,20] dendritic structures were studied, and in Refs. [45] it was shown that dendritic structures enhance the Raman signal more strongly in comparison with the particles. Although they can be inferior to other types in EF, in our opinion, SERS-active substrates based on arrays of nanoparticles are attractive because of their good controllability of the geometric parameters of particle ensembles [17,37,38] and the reproducibility of Raman signals, which is critical for practical use. Despite the higher average deviation due to the irregular shape, the obtained RSD values for the Ag–Cu particle array are close to pure Ag (<11%).The obtained RSD values (<11%) indicate a high integral homogeneity of SERS substrates (Fig. 9(d)). Similar RSD values using arrays of Ag–Cu particles were reported for other substances [25,30], while for Ag–Cu dendritic structures, the error values were significantly larger (~26.3%) [22].

4. Conclusion

To summarise, the arrays of Ag–Cu alloy nanoparticles were formed on the SiO_2 surface by vacuum-thermal evaporation of a small amount of substance and condensation on an unheated substrate, followed by low-temperature annealing at 230 °C. With the use of instrumental methods, it was found that Ag–Cu particles are formed as composites: part silver, part copper, and the Ag and Cu parts are necessarily in contact with each other, which corresponds to the eutectic nature of the Ag–Cu system. Such an array demonstrates a noticeable Raman signal amplification close in value to a similar array of pure silver nanoparticles. Moreover, if silver is characterized by a blue range, the maximum enhancement for the array of Ag–Cu particles shifts to the red region of the spectrum, but it turns out to be noticeably higher than for pure copper arrays. This is probably due to the difference in the plasma frequency of these metals, and to the fact that the resonant plasmon excited in the copper part of the particle propagates with less difficulty in the silver part of the particle, while when exposed to blue light, the resonant plasmon excited in the silver part of the particle will be damped in the copper part. Thus, the use of Ag–Cu nanoparticle arrays extends the spectral capabilities of SERS.

Declaration of competing interest

The authors declare that they have no known competing financial interests or personal relationships that could have appeared to influence the work reported in this paper.

CRediT authorship contribution statement

S.V. Dubkov: Writing - original draft, Supervision. **A.I. Savitskiy:**

Visualization. **A. Yu Trifonov:** Methodology. **G.S. Yeritsyan:** Investigation. **Yu.P. Shaman:** Data curation. **E.P. Kitsyuk:** Resources. **A. Tarasov:** Software. **O. Shtyka:** Validation. **R. Ciesielski:** Formal analysis. **D.G. Gromov:** Conceptualization, Writing - review & editing.

Acknowledgements

The work was supported by the Russian Science Foundation (Project No. 19-19-00595). XPS investigations were performed using equipment of the Joint Research Center «Material Science and Metallurgy» NUST MISIS. The authors thank E.A. Skryleva for help in interpreting the XPS results.

Appendix A. Supplementary data

Supplementary data to this article can be found online at https://doi.org/10.1016/j.omx.2020.100055.

References

[1] Z. Wang, H. Song, H. Pang, Y. Ning, T.D. Dao, Z. Wang, H. Chen, Y. Weng, Q. Fu, T. Nagao, Y. Fang, J. Ye, Photo-assisted methanol synthesis via CO2 reduction under ambient pressure over plasmonic Cu/ZnO catalysts, Appl. Catal. B Environ. 250 (2019) 10–16, https://doi.org/10.1016/j.apcatb.2019.03.003.

[2] F. Fathi, M.-R. Rashidi, Y. Omidi, Ultra-sensitive detection by metal nanoparticles-mediated enhanced SPR biosensors, Talanta 192 (2019) 118–127, https://doi.org/10.1016/j.talanta.2018.09.023.

[3] A.K. Pal, D. Bharathi Mohan, SERS enhancement, sensitivity and homogeneity studies on bi-metallic Ag-Cu films through tuning of broad band SPR towards red region, J. Alloys Compd. 698 (2017) 460–468, https://doi.org/10.1016/j.jallcom.2016.12.246.

[4] J.R. McLaughlan, Controllable nucleation of cavitation from plasmonic gold nanoparticles for enhancing high intensity focused ultrasound applications, JoVE (2018), https://doi.org/10.3791/58045.

[5] P. Shamjid, T. Abhijith, P. Vivek, C.S. Joel, V.S. Reddy, Plasmonic effects of Ag nanoparticles for absorption enhancement in polymer solar cells with MoO3 passivation layer, Phys. B Condens. Matter 560 (2019) 174–184, https://doi.org/10.1016/j.physb.2019.01.052.

[6] H.S. Kim, S.H. Lee, I. Choi, On-chip plasmonic immunoassay based on targeted assembly of gold nanoplasmonic particles, The Analyst 144 (2019) 2820–2826, https://doi.org/10.1039/C8AN02489H.

[7] A. Purwidyantri, C.-H. Hsu, C.-M. Yang, B.A. Prabowo, Y.-C. Tian, C.-S. Lai, Plasmonic nanomaterial structuring for SERS enhancement, RSC Adv. 9 (2019) 4982–4992, https://doi.org/10.1039/C8RA10656H.

[8] T.P. Araujo, J. Quiroz, E.C.M. Barbosa, P.H.C. Camargo, Understanding plasmonic catalysis with controlled nanomaterials based on catalytic and plasmonic metals, Curr. Opin. Colloid Interface Sci. 39 (2019) 110–122, https://doi.org/10.1016/j.cocis.2019.01.014.

[9] A. Otto, Surface-enhanced Raman scattering: “classical” and “chemical” origins, in: M. Cardona, G. Güntherodt (Eds.), Light Scattering in Solids IV, Springer Berlin Heidelberg, Berlin, Heidelberg, 1984, pp. 289–418. http://link.springer.com/10.1007/3-540-11942-6_24. (Accessed 3 July 2019).

[10] S.K. Maurya, S.P. Tiwari, A. Kumar, K. Kumar, Plasmonic enhancement of upconversion emission in Ag@NaYF4:Er3+/Yb3+ phosphor, J. Rare Earths 36 (2018) 903–910, https://doi.org/10.1016/j.jre.2018.03.003.

[11] M.S.A. MohdSaidi, S.K. Ghoshal, K. Hamzah, R. Arifin, M.F. Omar, M.K. Roslan, E. S. Sazali, Visible light emission from Dy3+ doped tellurite glass: role of silver and titania nanoparticles co-embedment, J. Non-Cryst. Solids 502 (2018) 198–209, https://doi.org/10.1016/j.jnoncrysol.2018.09.012.

[12] J.L. Montaño-Priede, O. Peña-Rodríguez, U. Pal, Near-electric-field tuned PlasmonicAu@SiO2 and Ag@SiO2 nanoparticles for efficient utilization in luminescence enhancement and surface-enhanced spectroscopy, J. Phys. Chem. C 121 (2017) 23062–23071, https://doi.org/10.1021/acs.jpcc.7b07395.

[13] K. Qian, B.C. Sweeny, A.C. Johnston-Peck, W. Niu, J.O. Graham, J.S. DuChene, J. Qiu, Y.-C. Wang, M.H. Engelhard, D. Su, E.A. Stach, W.D. Wei, Surface plasmon-driven water reduction: gold nanoparticle size matters, J. Am. Chem. Soc. 136 (2014) 9842–9845, https://doi.org/10.1021/ja504097v.

[14] A.G.M. da Silva, T.S. Rodrigues, J. Wang, L.K. Yamada, T.V. Alves, F.R. Ornellas, R. A. Ando, P.H.C. Camargo, The fault in their shapes: investigating the surface-plasmon-resonance-mediated catalytic activities of silver quasi-spheres, cubes, triangular prisms, and wires, Langmuir 31 (2015) 10272–10278, https://doi.org/10.1021/acs.langmuir.5b02838.

[15] S. Mukherjee, L. Zhou, A.M. Goodman, N. Large, C. Ayala-Orozco, Y. Zhang, P. Nordlander, N.J. Halas, Hot-electron-induced dissociation of H 2 on gold nanoparticles supported on SiO2, J. Am. Chem. Soc. 136 (2014) 64–67, https://doi.org/10.1021/ja411017b.

[16] V.S. Gorelik, Notes on the history of studies of Raman scattering at the P.N. Lebedev physical institute, J. Russ. Laser Res. 19 (1999) 513–527, https://doi.org/10.1007/BF02559661.

[17] D.G. Gromov, S.V. Dubkov, A.I. Savitskiy, Y.P. Shaman, A.A. Polokhin, I. A. Belogorokhov, A.Y. Trifonov, Optimization of nanostructures based on Au, Ag, Au-Ag nanoparticles formed by thermal evaporation in vacuum for SERS applications, Appl. Surf. Sci. 489 (2019) 701–707, https://doi.org/10.1016/j.apsusc.2019.05.286.

[18] S. Dubkov, A. Trifonov, Y. Shaman, E. Kitsyuk, A. Savitskiy, A. Polokhin, D. Gromov, SERS of a-C thin film on Ag, Au, Ag0.52-Au0.48 alloy nanoparticle arrays with normal particles size distribution formed by vacuum thermal evaporation, Defect Diffusion Forum 386 (2018) 250–255, https://doi.org/10.4028/www.scientific.net/DDF.386.250.

[19] S.-S. Chen, X.-X. Lin, A.-J. Wang, H. Huang, J.-J. Feng, Facile synthesis of multi-branched AgPt alloyed nanoflowers and their excellent applications in surface enhanced Raman scattering, Sensor. Actuator. B Chem. 248 (2017) 214–222, https://doi.org/10.1016/j.snb.2017.03.129.

[20] J.-J. Feng, X.-X. Lin, S.-S. Chen, H. Huang, A.-J. Wang, Thymine-directed synthesis of highly branched gold-palladium alloy nanobrambles as a highly active surface-enhanced Raman scattering substrate, Sensor. Actuator. B Chem. 247 (2017) 490–497, https://doi.org/10.1016/j.snb.2017.03.053.

[21] D. Li, J. Liu, H. Wang, C.J. Barrow, W. Yang, Electrochemical synthesis of fractal bimetallic Cu/Ag nanodendrites for efficient surface enhanced Raman spectroscopy, Chem. Commun. 52 (2016) 10968–10971, https://doi.org/10.1039/C6CC05215K.

[22] K. Chang, H. Chung, Simple electrochemical synthesis of an Au–Ag–Cu trimetallic nanodendrite and its use as a SERS substrate, RSC Adv. 6 (2016) 75943–75950, https://doi.org/10.1039/C6RA01670G.

[23] Z.-Q. Cheng, Z.-W. Li, R. Yao, K.-W. Xiong, G.-L. Cheng, Y.-H. Zhou, X. Luo, Z.-M. Liu, Improved SERS performance and catalytic activity of dendritic Au/Ag bimetallic nanostructures based on Ag dendrites, Nanoscale Research Letters 15 (2020), https://doi.org/10.1186/s11671-020-03347-4.

[24] X.-Y. Zhu, A.-J. Wang, S.-S. Chen, X. Luo, J.-J. Feng, Facile synthesis of AgPt@Ag core-shell nanoparticles as highly active surface-enhanced Raman scattering substrates, Sensor. Actuator. B Chem. 260 (2018) 945–952, https://doi.org/10.1016/j.snb.2017.12.185.

[25] M.S. Satya Bharati, B. Chandu, S.V. Rao, Explosives sensing using Ag–Cu alloy nanoparticles synthesized by femtosecond laser ablation and irradiation, RSC Adv. 9 (2019) 1517–1525, https://doi.org/10.1039/C8RA08462A.

[26] J.-P. Lee, D. Chen, X. Li, S. Yoo, L.A. Bottomley, M.A. El-Sayed, S. Park, M. Liu, Well-organized raspberry-like Ag@Cu bimetal nanoparticles for highly reliable and reproducible surface-enhanced Raman scattering, Nanoscale 5 (2013) 11620, https://doi.org/10.1039/c3nr03363e.

[27] K. Shin, D.H. Kim, S.C. Yeo, H.M. Lee, Structural stability of AgCu bimetallic nanoparticles and their application as a catalyst: a DFT study, Catal. Today 185 (2012) 94–98, https://doi.org/10.1016/j.cattod.2011.09.022.

[28] S. Dubkov, D. Gromov, A. Savitskiy, A. Trifonov, S. Gavrilov, Alloying effects at bicomponent Au-Cu and In-Sn particle arrays formation by vacuum-thermal evaporation, Mater. Res. Bull. 112 (2019) 438–444, https://doi.org/10.1016/j.materresbull.2018.10.003.

[29] Y. He, R. Wang, C. Sun, S. Liu, J. Zhou, L. Zhang, T. Jiao, Q. Peng, Facile synthesis of self-assembled NiFe layered double hydroxide-based azobenzene composite films with photoisomerization and chemical gas sensor performances, ACS Omega 5 (2020) 3689–3698, https://doi.org/10.1021/acsomega.9b04290.

[30] X. Yan, M. Wang, X. Sun, Y. Wang, G. Shi, W. Ma, P. Hou, Sandwich-like Ag@Cu@CW SERS substrate with tunable nanogaps and component based on the Plasmonic nanonodule structures for sensitive detection crystal violet and 4-aminothiophenol, Appl. Surf. Sci. 479 (2019) 879–886, https://doi.org/10.1016/j.apsusc.2019.02.072.

[31] P.R. Subramanian, J.H. Perepezko, The Ag-Cu (silver-copper) system, J. Phase Equil. 14 (1993) 62–75, https://doi.org/10.1007/BF02652162.

[32] K.S. Tan, K.Y. Cheong, Advances of Ag, Cu, and Ag–Cu alloy nanoparticles synthesized via chemical reduction route, J. Nanoparticle Res. 15 (2013), https://doi.org/10.1007/s11051-013-1537-1.

[33] K.D. Malviya, K. Chattopadhyay, Synthesis and mechanism of composition and size dependent morphology selection in nanoparticles of Ag–Cu alloys processed by laser ablation under liquid medium, J. Phys. Chem. C 118 (2014) 13228–13237, https://doi.org/10.1021/jp502327c.

[34] J. Hu, Z. Wang, J. Li, Gold nanoparticles with special shapes: controlled synthesis, surface-enhanced Raman scattering, and the application in biodetection, Sensors 7 (2007) 3299–3311, https://doi.org/10.3390/s7123299.

[35] M.S. Rodrigues, D. Costa, R.P. Domingues, M. Apreutesei, P. Pedrosa, N. Martin, V. M. Correlo, R.L. Reis, E. Alves, N.P. Barradas, P. Sampaio, J. Borges, F. Vaz, Optimization of nanocomposite Au/TiO 2 thin films towards LSPR optical-sensing, Appl. Surf. Sci. 438 (2018) 74–83, https://doi.org/10.1016/j.apsusc.2017.09.162.

[36] D. Gromov, S. Dubkov, A. Savitskiy, Y. Grishina, V. Rubtsov, Investigation of Ag nanoparticles fusion process by subsequent vacuum thermal evaporation, in: IEEE Conference of Russian Young Researchers in Electrical and Electronic Engineering (EIConRus), IEEE, St. Petersburg and Moscow, Russia, 2017, pp. 1156–1159, https://doi.org/10.1109/EIConRus.2017.7910763, 2017.

[37] D.G. Gromov, L.M. Pavlova, A.I. Savitskii, A.Y. Trifonov, Investigation of the early stages of condensation of Ag and Au on the amorphous carbon surface during thermal evaporation under vacuum, Phys. Solid State 57 (2015) 173–180, https://doi.org/10.1134/S1063783415010126.

[38] D.G. Gromov, L.M. Pavlova, A.I. Savitsky, A.Y. Trifonov, Nucleation and growth of Ag nanoparticles on amorphous carbon surface from vapor phase formed by vacuum evaporation, Appl. Phys. A 118 (2015) 1297–1303, https://doi.org/10.1007/s00339-014-8834-0.

[39] B.M. Johnson, The use of radioactive microspheres to compare the effects of hydralazine, guanethidine and SK & F 24260 on the redistribution of cardiac output in anaesthetized rabbits, Br. J. Pharmacol. 55 (1975) 393–402, https://doi.org/10.1111/j.1476-5381.1975.tb06943.x.
[40] H. Kröger, I. Donner, G. Skiello, Influence of a new virostatic compound on the induction of enzymes in rat liver, Arzneimittelforschung 25 (1975) 1426–1429.
[41] A.C. Ferrari, J. Robertson, Interpretation of Raman spectra of disordered and amorphous carbon, Phys. Rev. B 61 (2000) 14095–14107, https://doi.org/10.1103/PhysRevB.61.14095.
[42] K.P. Rice, E.J. Walker, M.P. Stoykovich, A.E. Saunders, Solvent-dependent surface plasmon response and oxidation of copper nanocrystals, J. Phys. Chem. C 115 (2011) 1793–1799, https://doi.org/10.1021/jp110483z.
[43] G.H. Chan, J. Zhao, E.M. Hicks, G.C. Schatz, R.P. Van Duyne, Plasmonic properties of copper nanoparticles fabricated by nanosphere lithography, Nano Lett. 7 (2007) 1947–1952, https://doi.org/10.1021/nl070648a.
[44] B.N. Khlebtsov, V.A. Khanadeev, E.V. Panfilova, D.N. Bratashov, N.G. Khlebtsov, Gold nanoisland films as reproducible SERS substrates for highly sensitive detection of fungicides, ACS Appl. Mater. Interfaces 7 (2015) 6518–6529, https://doi.org/10.1021/acsami.5b01652.
[45] L.D. Rafailović, C. Gammer, J. Srajer, T. Trišović, J. Rahel, H.P. Karnthaler, Surface enhanced Raman scattering of dendritic Ag nanostructures grown with anodic aluminium oxide, RSC Adv. 6 (2016) 33348–33352, https://doi.org/10.1039/C5RA26632G.